Using Crosscorrelation to Mitigate Analog/RF Impairments for Integrated Spectrum Analyzers

Mark S. Oude Alink, *Student Member, IEEE*, Eric A. M. Klumperink, *Senior Member, IEEE*, André B. J. Kokkeler, Zhiyu Ru, *Member, IEEE*, Wei Cheng, and Bram Nauta, *Fellow, IEEE*

Abstract—An integrated spectrum analyzer is useful for built-in self-test purposes, software-defined radios, or dynamic spectrum access in cognitive radio. The analog/RF performance is impaired by a number of factors, including thermal noise, phase noise, and nonlinearity. In this paper, we present an integrated circuit with two integrated RF-frontends, of which the outputs are crosscorrelated in digital baseband. We show by theory and measurements that the above-mentioned impairments are mitigated by this technique. The presented 65-nm CMOS prototype operates at 1.2 V, and obtains a noise floor below -169 dBm/Hz, an IIP_3 of $+25$ dBm, and more than 20 dB of phase-noise reduction. In a special high-impedance mode, an even lower noise floor below -172 dBm/Hz is obtained.

Index Terms—Built-in self-test (BIST), cognitive radio, crosscorrelation, dynamic spectrum access, noise reduction, spectrum analyzer (SA), spectrum sensing.

I. INTRODUCTION

WIDEBAND integrated receivers for software-defined radios (SDRs) face several significant challenges due to the required wideband operation. Limited filtering before the signal enters the chip causes strong interferers in combination with the circuit's nonlinearity to create distortion products. These same interferers impose gain limitations on the receiver chain, causing thermal noise to degrade the performance as

M. S. Oude Alink is with the Computer Architecture for Embedded Systems (CAES) Group and the Integrated Circuit Design (IC-Design) Group, Centre for Telematics and Information Technology (CTIT), University of Twente, 7500 AE Enschede, The Netherlands (e-mail: m.s.oudealink@utwente.nl).

E. A. M. Klumperink and B. Nauta are with the Integrated Circuit Design (IC-Design) Group, Centre for Telematics and Information Technology (CTIT), University of Twente, 7500 AE Enschede, The Netherlands.

A. B. J. Kokkeler is with the Computer Architecture for Embedded Systems (CAES) Group, Centre for Telematics and Information Technology (CTIT), University of Twente, 7500 AE Enschede, The Netherlands.

Z. Ru was with the Integrated Circuit Design (IC-Design) Group, Centre for Telematics and Information Technology (CTIT), University of Twente, 7500 AE Enschede, The Netherlands. He is now with MediaTek, Woburn, MA 01801 USA.

W. Cheng was with the Integrated Circuit Design (IC-Design) Group, Centre for Telematics and Information Technology (CTIT), University of Twente, 7500 AE Enschede, The Netherlands. He is now with Qualcomm, San Diego, CA 92121 USA.

Color versions of one or more of the figures in this paper are available online at http://ieeexplore.ieee.org.
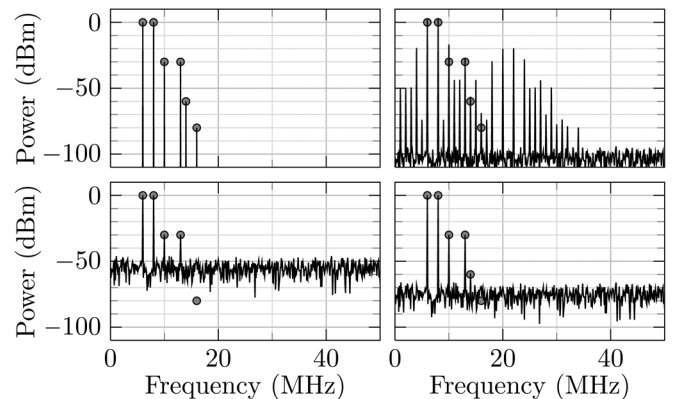
Fig. 1. Illustration of SFDR limitation due to noise and nonlinearity. The example SA has $NF = 20$ dB and $IIP_3 = +10$ dBm and uses $RBW = 100$ kHz. The true input powers are indicated by circles. (*top-left*) Input, (*top-right*) output with 0-dB attenuation, (*bottom-left*) output with 48-dB attenuation, and (*bottom-right*) output with 28-dB attenuation.

well. Furthermore, widely tunable frequency generation generally results in higher phase noise. Reciprocal mixing with strong interferers results in high noise levels.

An integrated spectrum analyzer (SA) could aid an SDR in reducing these problems. By identifying the frequency and power of signals in the spectrum, it can enable the SDR to optimally tune its settings, such as the choice of IF center frequency to avoid a difficult image problem, or to set the center frequency of a notch filter to notch out a large blocker [1], [2]. Moreover, an SA is indispensible for cognitive radio or dynamic spectrum access, where the paradigm is to choose the frequency band for communication based on locally and temporarily unused spectrum. The detection of very weak signals in the presence of strong signals in adjacent channels calls for a high dynamic range. An integrated SA can also measure and process the internal high-frequency signals for built-in self-test (BIST), including high dynamic-range tests such as measuring receiver IIP_3 or small in-band spurs of a transmitter. This can save on pin-count, expensive test time, and when used for self-calibration, more robustness over process, temperature, and process variations. Finally, an integrated SA can enable the production of lower cost laboratory equipment.

An integrated wideband SA will suffer from the same nonidealities as a wideband receiver. An illustration of the effects of two nonidealities, noise and nonlinearity, is given in Fig. 1. Six sinusoids, with a power ranging from -80 to 0 dBm, are applied to the input of the SA (top-left). An ideal SA would show this on its display. The example SA has a noise figure (NF) of 20 dB and a IIP_3 of $+10$ dBm, and its output spectrum is shown top-right. The displayed average noise level (DANL) per hertz bandwidth,

$\mathrm{DANL_{Hz}}$, is equal to $-174 + 20 = -154$ dBm/Hz so the DANL is -104 dBm for the resolution bandwidth (RBW) of 100 kHz in this example. The distortion products completely obscure the weak signals and appear as many additional relatively strong signals. These can be reduced with attenuation at the input, as shown bottom-left. Unfortunately, the DANL is now higher than the weakest signals, thus they are still difficult to detect. The optimum is found with the strongest distortion component roughly at the level of the DANL (bottom-right). The required attenuation can be easily calculated: referred to the input, 1 dB of attenuation increases the DANL by 1 dB and reduces the third-order distortion components by 2 dB.

Still, the weakest signal is below the DANL. The RBW defines the frequency resolution; the higher it is, the more noise is present (assuming white noise), and thus the higher the DANL will be. Thus, for a sinusoid, lowering the RBW helps. The strongest and weakest signal that can be detected at the same time is indicated by the spurious-free dynamic range (SFDR), which can be formulated as (assuming it is limited by noise and $\mathrm{IIP_3}$) [3]

$$\mathrm{SFDR} = \frac{2}{3}(\mathrm{IIP_3} - \mathrm{DANL_{Hz}} - 10\log_{10}\mathrm{RBW}) \qquad (1)$$

where $\mathrm{IIP_3}$ is specified in dBm, $\mathrm{DANL_{Hz}}$ in dBm/Hz, and RBW in Hz. For the example SA, the SFDR is 76 dB, which is below the required 80 dB. A sinewave has a bandwidth of 0 Hz so the RBW can be lowered to improve the SNR. For other signals, lowering the RBW has a limit: at some point both the noise power and signal power decrease.

An SA does, however, have one advantage: it does not have to demodulate the received signals. This gives a degree of freedom, which is exploited in this work to improve the SFDR. In [3], we introduced the concept of crosscorrelation to improve linearity and reduce thermal and phase noise of an SA. The basic principle is to split the input signal, use two receivers and crosscorrelate their outputs to arrive at a power estimate. With identical input signals, but independent noise contributions, the noise averages out and the signal remains.

In this paper, we present a prototype with fully integrated RF-frontends exploiting this crosscorrelation concept. Parts of this work have been presented in [4], but here we add additional measurements, implementation details and analyses. We also present an additional unmatched (or "highZ") mode for better noise performance. When crosscorrelation spectrum sensing is not required, the second receiver may simply be turned off. Alternatively, each receiver may be connected to individual antennas for multiple-input multiple-output (MIMO) reception or to receive a separate band. Therefore, measurement results of a single receiver are also presented.

In Section II, we describe the principle of crosscorrelation spectrum sensing and how crosscorrelation can be used to alleviate the analog impairments. Section III describes our implementation in detail, followed by measurement results in Section IV. We end with conclusions in Section VI.

II. CROSSCORRELATION SPECTRUM SENSING

The key concern is measuring the power of an unknown signal in a certain frequency band. The principle of power
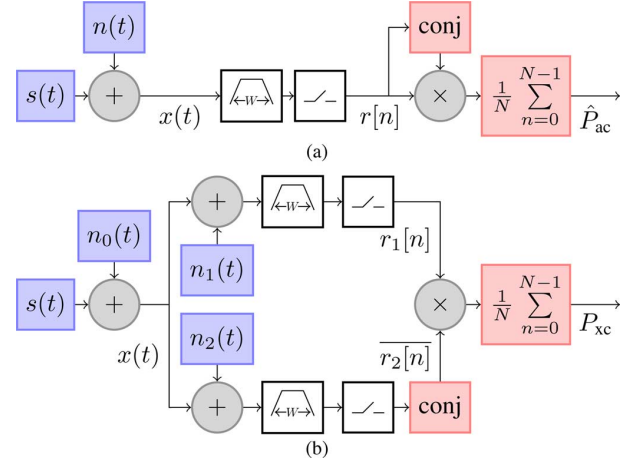

Fig. 2. Crosscorrelation system is a generalization of a standard SA. (a) Block diagram of an SA (one receiver). (b) Block diagram for crosscorrelation (two receivers).

detection in an SA is first discussed in Section II-A, after which the principle of crosscorrelation spectrum sensing is explained in Section II-B. We then discuss how crosscorrelation can be used to improve linearity in Section II-C and phase noise in Section II-D.

A. Power Detection in an SA

A block diagram of an SA is shown in Fig. 2(a). The receiver chain, which typically includes an antenna that picks up signal $s(t)$, a low-noise amplifier (LNA), a mixer, some amplifiers and filters, and an analog-to-digital converter (ADC), is modeled as a device that only adds some noise (frequency translation and phase shifts are ignored in this model). The combination of s (with power P_s) and (input-referred) noise n (with power P_n) is denoted as x. This x is filtered in each path by a filter with bandwidth W and then sampled at the Nyquist rate, resulting in the complex receiver output r. The power is estimated by $\hat{P}_{\mathrm{ac}} \triangleq \frac{1}{N}\sum_{n=0}^{N-1}|r[n]|^2$. This is a form of autocorrelation, as the output signal is being correlated with itself; hence, the "ac" subscript. Note that $|r[n]|^2 = r[n]\overline{r[n]}$ with $\overline{r[n]}$ being the complex conjugate of $r[n]$. The complex conjugate ("conj") block is explicitly shown in Fig. 2(a) to illustrate the similarities with Fig. 2(b).

The measurement variance is proportional to $\frac{1}{N}(P_s + P_n)^2$. A large variance obscures small signals so N should be large enough to reduce the variance. The DANL is the average noise level as would be displayed on the screen of an SA, and is thus equal to $\mathbb{E}[\hat{P}_{\mathrm{ac}}] = P_s + P_n$.

The power of the noise can be estimated and subtracted from the measured results, but the estimation will always have some error and device noise changes over time, frequency, and with temperature.[1] This means that weak signals below a certain SNR will not be detectable, even for infinite measurement time. In the context of cognitive radio, this minimum signal-to-noise ratio (SNR) is called the SNR wall, a term coined by Tandra and Sahai [5].

---

[1]In the Agilent PXA spectrum analyzer, the so-called noise floor extension (NFE) does exactly this. With NFE turned on, $\mathrm{DANL_{Hz}}$ reduces from -154 to -162 dBm/Hz at room temperature. If the estimation were perfect, it would be reduced to the thermal noise of the matched input source: -174 dBm/Hz.
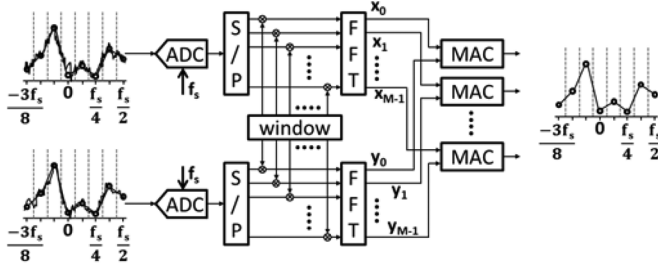
Fig. 3. When the ADCs can sample sufficiently fast, multiple channels may be processed simultaneously in the digital domain, e.g., by using FFTs (and windowing). The multiply-accumulate (MAC) blocks perform the multiplication and summation, as depicted in separate blocks in Fig. 2(b).

A fast Fourier transform (FFT) (or other digital signal processing (DSP) techniques) may be employed in the digital domain to simultaneously sense multiple channels within this bandwidth W, as shown in Fig. 3. This allows low-cost flexible spectrum analysis, as the RBW can be easily changed by using a (windowed) M-point FFT to divide the bandwidth W into M subbands of W/M Hz. With rectangular windowing and using nonoverlapping FFTs, each subband will have N/M independent samples available.

B. Principle of Crosscorrelation Spectrum Sensing

In [6], it is shown that crosscorrelation can lower the SNR wall without degrading linearity, thus allowing signals at smaller SNR to be detected. The basic principle is depicted in Fig. 2(b). The input signal is split and processed by two separate, but otherwise identical receivers, each of which adds its own independent noise (n_1 and n_2, respectively, with $P_{n_1} = P_{n_2}$) to the input signal. The splitter (and possibly subsequent components) may introduce some noise that is present in both receivers, and can thus be referred to the input as n_0. The receiver outputs r_1 and r_2 are combined as

$$P_{\mathrm{xc}} \triangleq \frac{1}{N} \sum_{n=0}^{N-1} r_1[n]\overline{r_2[n]}. \tag{2}$$

where $\overline{r_2}$ denotes the complex conjugate of r_2, and N the number of complex samples taken. The subscript xc is used to indicate its relation with crosscorrelation. With $\hat{P}_{\mathrm{xc}} \triangleq \mathcal{R}(P_{\mathrm{xc}})$, where $\mathcal{R}(\cdot)$ takes the real part [6]

$$\mathbb{E}[\hat{P}_{\mathrm{xc}}] = P_s + P_{n_0}$$
$$\mathrm{var}[\hat{P}_{\mathrm{xc}}] \approx \frac{1}{N}\left(\left(P_s + P_{n_0} + \frac{1}{2}P_{n_1}\right)^2 + \frac{1}{4}P_{n_1}^2\right). \tag{3}$$

Any uncertainty in P_{n_1} and P_{n_2} only influences the variance, which is reduced by increasing the measurement time. Thus, in going from Fig. 2(a) to Fig. 2(b), as much as possible of n should be moved to n_1 and n_2, and as little as possible to n_0. With crosscorrelation, the final DANL of the SA can be much lower, as P_{n_0} can be much lower than P_n.

In a practical implementation, the receivers will contain one or more mixers to perform frequency conversion, and local oscillators (LOs) to drive these mixers. The phase of the LO is transferred to the frequency-converted output of the mixer so any phase difference that may exist between the LOs of the

two receivers will directly cause a phase difference of the input signal at the two receiver outputs. Moreover, practical nonidealities, such as asymmetry in the splitter or mismatch in component values, may introduce a phase shift between the two receivers. For the desired signal component, $r_2[n] = r_1[n] \cdot \exp(j2\pi n\Delta\phi/f_s)$, resulting in loss of signal power. A simple solution is to take $\tilde{P}_{\mathrm{xc}} \triangleq |P_{\mathrm{xc}}|$ as metric, which is done in this work. The statistics then become (with κ_μ and κ_{σ^2} being long expressions involving the signal and noise components) [6]

$$\mathbb{E}[\tilde{P}_{\mathrm{xc}}] \approx \sqrt{(P_s + P_{n_0})^2 + \frac{\kappa_\mu}{N}}$$
$$\mathrm{var}[\tilde{P}_{\mathrm{xc}}] \approx \frac{1}{N}\left((P_s + P_{n_0})^2 + \kappa_{\sigma^2}\right). \tag{4}$$

The DANL ($\mathbb{E}[\tilde{P}_{\mathrm{xc}}]$) converges for large N to $P_s + P_{n_0}$.

C. Linearity Improvement

At some point, the first stage (which is often an LNA) will limit the total linearity. A way to increase linearity then is to attenuate the input signal, which is also what is done in commercial SAs. We assume a matched system with resistive attenuators so the NF of the attenuator is equal to its loss in dB. Similarly, IIP_3 (in dB) is improved by the attenuator loss.

From Fig. 2(b), it follows that if the attenuator is placed directly behind the antenna, all its noise will be present in both receivers. If it is placed *after* the splitter, it turns out that n_0 remains unaffected, as derived in [3]. In principle, the linearity can be arbitrarily increased without affecting the DANL, but 3 dB more attenuation requires a $4\times$ longer measurement time.

D. Phase-Noise Reduction

Phase noise manifests itself mostly around strong input signals via reciprocal mixing, thereby obscuring weak signals in the vicinity. Similar to thermal noise, phase noise can be reduced by crosscorrelation at the cost of measurement time. It requires each receiver to employ a separate oscillator, as is also done in some professional phase-noise analysis devices [7]. Their phase noise will be uncorrelated, apart from the phase noise of a common (external) reference (the generators need to be frequency locked), which can be very low.

III. IMPLEMENTATION

An implementation exploiting crosscorrelation needs two linear receivers, with an attenuator for each receiver to boost linearity. The attenuator should have low insertion loss (IL) in its bypass state to not degrade NF more than necessary.

The passive mixer-first architecture used in [3] lacks isolation between the front-ends, which limits the obtainable phase noise reduction. It also prohibits the use of a frequency offset between the two receivers, which is useful when two bands should be received simultaneously, or harmonic rejection (HR) techniques employing crosscorrelation are required [8]. A solution is provided by [9], where the voltage swings are kept low at RF to improve linearity. At baseband, feedback techniques can improve linearity to handle voltage swings.

Fig. 4 shows the system diagram with the parts that are implemented on-chip in the dashed box. In our implementation, the
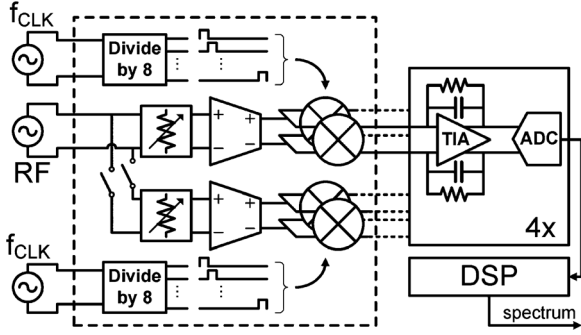
Fig. 4. System diagram of the proposed system with the dashed box indicating the parts integrated on-chip.
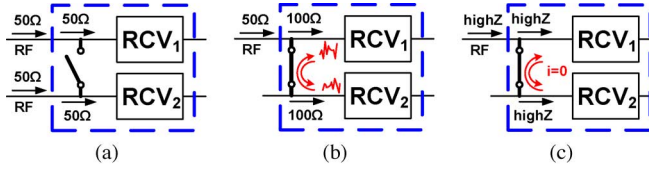

Fig. 5. Chip can be reconfigured to several modes. (a) Single-receiver mode. (b) Matched mode. (c) HighZ mode.

attenuator is followed by a low-noise transconductance amplifier (LNTA) for input power to current conversion. The output current of the LNTA is then mixed down by a passive mixer employing an HR architecture. Following circuitry is left off-chip to allow for more experimental freedom and to more easily measure the achieved RF linearity.

A transimpedance amplifier (TIA) with RC feedback at the baseband is used to convert the current to a voltage, while at the same time providing a first-order low-pass filter to limit the IF bandwidth. This low-pass filtering will attenuate blockers before they generate a large swing, thus improving overall linearity. The inputs of the TIA (implemented with a TI-THS4130 opamp) act as a virtual ground, reducing the swing at the output of the LNTA, improving its linearity. The TIAs are followed by more amplification to properly interface with the ADCs, which are preceded by antialias filters.

When not used for crosscorrelation spectrum sensing, both receivers may be operating standalone. A switch is then required to (dis)connect them. This gives the configurations in Fig. 5(a) and (b); how to implement the change in impedance is discussed later. Furthermore, we have implemented a mode where both receivers have a high-ohmic input impedance, referred to as "highZ," as shown in Fig. 5(c). The reason for this mode will be explained in more detail in Section II-B.

A. Attenuator

The attenuator is used to improve the linearity of the receiver, while the additional noise is reduced through crosscorrelation. Thus, the attenuator should not limit linearity itself. We assume that both the attenuator and receiver are in the weakly nonlinear region with only odd-order distortion

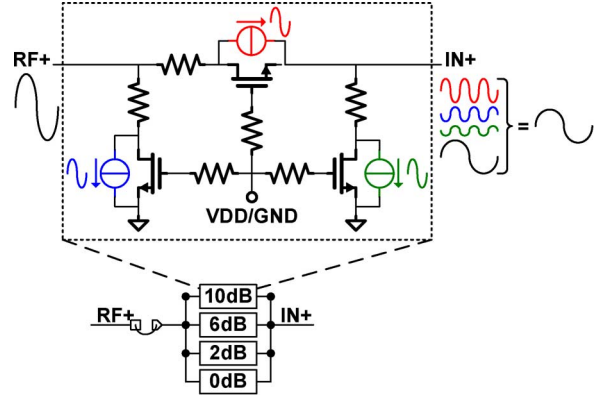$$y_{att}(x) \approx a_1 x + a_3 x^3 \quad y_{rcv}(x) \approx b_1 x + b_3 x^3. \quad (5)$$

Fig. 6. Circuit-level implementation of the attenuator. Correct sizing of the transistors cancels the third-order nonlinearity of the on-resistance.

$\mathrm{IIP}_{3,att}$ (in V^2) of the attenuator is $4/3|a_1/a_3|$, and $\mathrm{IIP}_{3,rcv}$ is $4/3|b_1/b_3|$. Then

$$y_{rcv}(y_{att}(x)) \approx a_1 b_1 x + (b_1 a_3 + b_3 a_1^3) x^3. \quad (6)$$

Thus, $\mathrm{IIP}_{3,cascade} = 4/3|a_1 b_1/(b_1 a_3 + b_3 a_1^3)|$. An ideal attenuator has $a_3 = 0$ such that $\mathrm{IIP}_{3,cascade}$ is $4/3|(b_1/b_3)/a_1^2|$. In other words, $\mathrm{IIP}_{3,cascade} = \mathrm{IIP}_{3,rcv} + A$ dB with $A = 1/a_1^2$ being the attenuation in dB. To calculate the allowable a_3, and thus the required $\mathrm{IIP}_{3,att}$, we solve (with δ being the allowable deterioration of $\mathrm{IIP}_{3,cascade}$ as compared to an ideal attenuator)

$$\frac{a_1 b_1}{b_1 a_3 + b_3 a_1^3} > \delta \frac{b_1}{a_1^2 b_3} \Rightarrow \frac{a_1}{a_3} > \frac{1}{a_1^2} \cdot \frac{b_1}{b_3} \cdot \frac{\delta}{1-\delta}. \quad (7)$$

Here we assumed a compressive nonlinearity, where a_3 (b_3) has the opposite sign from a_1 (b_1). For 1 dB of allowed deterioration ($\delta \approx 0.8$), $\mathrm{IIP}_{3,att} > \mathrm{IIP}_{3,rcv} + A + 6$ (dBm). If $\mathrm{IIP}_{3,rcv} = 15$ dBm and $A = 10$ dB, $\mathrm{IIP}_{3,att} > 31$ dBm is required.

A resistor ladder would be most linear with an LNTA attached to each node. This consumes a lot of area and is not suitable for our LNTA topology. Thus, an attenuator is desired that functions as a two-port, with one matched input and one matched output. This can be obtained by a Π-attenuator configuration, as shown in Fig. 6.

Several settings are implemented (single ended) with 2-, 6-, and 10-dB attenuation. The resistors in series with the gate improve bandwidth and reduce the effect of the nonlinear capacitance [10]. The transistors are sized such that the third-order distortion from the series transistor is to a large degree canceled by the third-order distortion of the parallel transistors. This technique achieves high linearity with small switches for improved bandwidth and less feedthrough, and is described in more detail in [10]. An additional large bypass switch is added as a 0-dB setting; it gives only 0.1-dB IL.

The input impedance needs to be 50 Ω when the receiver is used for regular reception, and 100 Ω when two receivers are put in parallel for crosscorrelation spectrum sensing. Therefore, each setting is designed for 100-Ω input and output matching, and two of them are put in parallel to enable 50-Ω input matching.
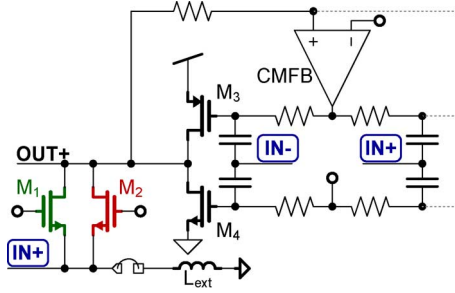
Fig. 7. Circuit-level implementation of one LNTA slice (half-circuit shown).
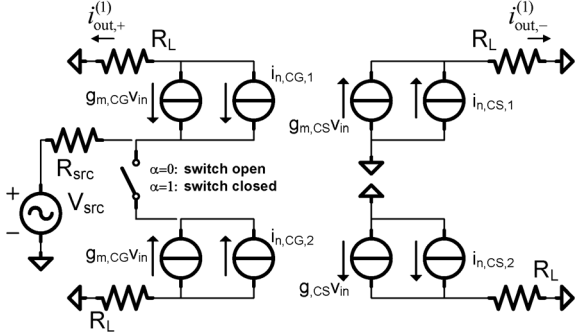

Fig. 8. Small-signal equivalent circuit for LNTA noise analysis in all modes.

B. LNTA

The LNTA consists of seven identical fully differential slices. It has a differential input and is based on the design of [9]. A half-circuit of one slice is shown in Fig. 7. The seven slices of the LNTA are combined in a 2:3:2 ratio to approximate the ideal $1:\sqrt{2}:1$ ratio of an HR mixer to suppress the third and fifth harmonic of the square-wave LOs.[2]

A common-gate (CG) stage (M_1 and M_2) provides matching: each transistor has $g_m \approx 1.4$ mS so with seven slices in parallel, this amounts to $R_{\text{in}} \approx 1/(7 \cdot 2 \cdot 1.4 \cdot 10^{-3}) \approx 50 \ \Omega$. By selectively turning zero, one or two transistors on per slice, a highZ, 100- or 50-Ω input impedance can be obtained, respectively. The common-mode feedback (CMFB) circuit makes sure that the output remains biased at half the supply voltage to enable maximum output swing. A common-source (CS) stage [M_3 ($g_m \approx 6.8$ mS) and M_4 ($g_m \approx 4.8$ mS)] provides additional gain. M_3 provides the bias current for M_1 and M_2, which is shunted by the external inductor of 100 nH that is shared by all slices.

The CG-CS configuration has the ability to cancel the noise of the CG stage if their gain has the same magnitude, but opposite phase [14]. In our implementation $g_{m,\text{CS}} \gg g_{m,\text{CG}}$ so the cancellation is only partial. For the noise analysis, we consider the transistors as ideal voltage-controlled current sources with noise power spectral density (PSD) equal to $4kT\gamma g_m$ W/Hz, with γ being the noise excess factor of the transistor (usually somewhere between 2/3 and 3/2). A small-signal equivalent circuit is shown in Fig. 8.

---

[2]An HR mixer removes certain harmonics of its LO by summing properly amplified versions of the input signal with properly phase-shifted versions of the LO. It is a commonly used technique in wideband receivers, see e.g., [9], [11]–[13].

Define $g_{m,\text{CG}} \triangleq 7(g_{m,M_1} + g_{m,M_2})$, $g_{m,\text{CS}} \triangleq 7(g_{m,M_3} + g_{m,M_4}) \approx 80$ mS, $g_{m,\text{tot}} \triangleq g_{m,\text{CG}} + g_{m,\text{CS}}$. With crosscorrelation, two LNTAs will be in parallel: define $\alpha = 1$ in that case, and define $\alpha = 0$ when the two receivers are disconnected. The output current of the first receiver $i_{\text{out}}^{(1)}$ is equal to

$$
\begin{aligned}
i_{\text{out}}^{(1)} &= i_{\text{out},+}^{(1)} - i_{\text{out},-}^{(1)} \\
&= H_{n,\text{src}}^{(1)} i_{n,\text{src}} + H_{n,\text{CG},1}^{(1)} i_{n,\text{CG},1} + H_{n,\text{CG},2}^{(1)} i_{n,\text{CG},2} \\
&\quad + H_{n,\text{CS},1}^{(1)} i_{n,\text{CG},1} + H_{n,\text{CS},2}^{(1)} i_{n,\text{CG},2}
\end{aligned}
\tag{8}
$$

with $H_{xx}^{(1)}$ being the transfer from noise current i_{xx} to $i_{\text{out}}^{(1)}$, which can be easily derived from the small-signal equivalent circuits. Note that with our approximations, $H_{n,\text{CS},2} = 0$, and when $\alpha = 0$, $H_{n,\text{CG},2} i_{n,\text{CG},2} = 0$. The following expression for the noise factor can then be obtained:

$$
\begin{aligned}
F = 1 &+ \gamma_{m,\text{CG}} \frac{(1 + (\alpha g_{m,\text{CG}} - g_{m,\text{CS}})R_{\text{src}})^2}{g_{m,\text{tot}}^2 R_{\text{src}}} \\
&+ \gamma g_{m,\text{CS}} \frac{(1 + (1+\alpha)g_{m,\text{CG}}R_{\text{src}})^2}{g_{m,\text{tot}}^2 R_{\text{src}}} + \alpha \gamma g_{m,\text{CG}} R_{\text{src}}.
\end{aligned}
\tag{9}
$$

For $\gamma \approx 1$, the NF in 50-Ω mode ($g_{m,\text{CG}} \approx 20$ mS) is 3.0 dB. In 100-Ω mode ($g_{m,\text{CG}} \approx 10$ mS), when the other receiver is connected and in 100-Ω mode as well, the NF is 3.8 dB. In the highZ mode ($g_{m,\text{CG}} = 0$), it results in a NF of only 1.0 dB. This is all within 0.1 dB from simulation results.

Part of the LNTA and the following stages contribute independent noise in the individual receivers so, at this point, we can calculate the DANL expected after crosscorrelation. We are interested in the product of the receiver outputs, as this is effectively the used PSD estimate using crosscorrelation [see (2)]. By noting that crossterms involving noise components from different devices have an expectation of 0, we can find

$$
\begin{aligned}
\mathbb{E}\left[i_{\text{out}}^{(1)} \overline{i_{\text{out}}^{(2)}}\right] = |H_{n,\text{src}}^2|^2 \mathbb{E}\left[i_{n,\text{src}}^2\right] &+ H_{n,\text{CG},1}^{(1)} \overline{H_{n,\text{CG},1}^{(2)}} \\
\times \mathbb{E}\left[i_{n,\text{CG},1}^2\right] + H_{n,\text{CG},1}^{(1)} \overline{H_{n,\text{CG},2}^{(2)}} &\mathbb{E}\left[i_{n,\text{CG},2}^2\right].
\end{aligned}
\tag{10}
$$

Due to symmetry, $H_{n,\text{CG},1}^{(1)} = H_{n,\text{CG},2}^{(2)}$, $H_{n,\text{CG},2}^{(1)} = H_{n,\text{CG},1}^{(2)}$, etc. Using $\mathbb{E}[i_{n,\text{src}}^2] = 4kT/R_{\text{src}}$, $\mathbb{E}[i_{n,\text{CG},1}^2] = \mathbb{E}[i_{n,\text{CG},2}^2] = 4kT\gamma g_{m,\text{CG}}$, and the fact that the transfers are in the idealized situation not frequency dependent, it is possible to find a "correlated noise factor" similar to (9),

$$
F_{\text{corr}} = 1 + 2 \frac{H_{n,\text{CG},1}^{(1)} H_{n,\text{CG},1}^{(2)}}{|H_{n,\text{src}}|^2} \gamma g_{m,\text{CG}} R_{\text{src}}.
\tag{11}
$$

The result is that for $\gamma \approx 1$, $\text{NF}_{\text{corr}} = 2.0$ dB in the 100-Ω mode. In other words, after crosscorrelation for long enough time, DANL_{Hz} should converge to -172 dBm/Hz. The residual noise correlation is caused by the CG-noise currents flowing between the two receivers, as is illustrated in Fig. 5(b).

From (11), it is clear that if $g_{m,\text{CG}} = 0$, $F_{\text{corr}} = 1$, and thus, $\text{NF}_{\text{corr}} = 0$. This is the case for the highZ mode: Fig. 5(c) illustrates this effect by showing zero current flow between the two receivers, compared to nonzero current flow in the 100-Ω mode. After long enough crosscorrelation, *all* receiver noise
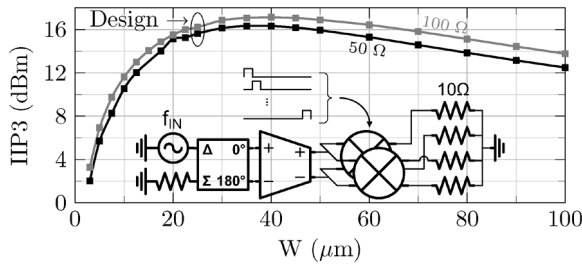
Fig. 9. IIP_3 simulation of cascade of LNTA and mixer at $f_{\text{LO}} = 500$ MHz.

is removed, and only the noise from the source will remain: DANL_{Hz} will be equal to -174 dBm/Hz.

C. Mixer and LO

An externally applied clock is divided by 8 to generate an eight-phase LO with 1/8 duty cycle at an eight times lower frequency. This eight-phase LO drives the HR mixer, which steers the LNTA outputs currents to a differential in-phase/quadrature (I/Q) output.

Fig. 9 shows a plot of IIP_3 for the cascade of LNTA and passive mixer (driven by an ideal LO), where the width of the mixer switches is swept. The impedance from mixer output to TIA input and the nonideality of the TIA are simulated as an ideal 10-Ω resistance (IIP_3 is determined at these 10-Ω resistors). Larger mixer switches require a more power-hungry clock driver so a width of 25 μm is used to obtain a simulated IIP_3 of around $+16$ dBm for the cascade, in both 50- and 100-Ω mode. In both cases, the choice is less than 1 dB from the simulated optimum at a width of 40 μm.

The LO-generation circuitry is shown in Fig. 10. It first converts a differential sine-wave input to a square wave, which is then used to drive a circular shift register. One flipflop is preloaded with a "1", and all others with "0". In this way, the eight outputs have a duty cycle of 1/8. The maximum input frequency is 8 GHz (limited by the reset circuitry) so the maximum LO frequency is 1 GHz.

The shift-register outputs are buffered by clock drivers to drive the mixer switches. A small overlap of the clock phases, which can occur due to mismatch, can result in significant noise degradation. Therefore, the clock drivers internally employ asymmetric rise and fall times to slightly reduce the duty cycle to nominally 1/9.

D. On-Chip Receiver Connection

The two receivers on-chip are identical. For easier printed circuit board (PCB) routing (one differential transmission line per side), the second receiver is rotated 180° with respect to the other (no strict receiver matching is required [3]). This requires a long on-chip wire (>1 mm) to connect them, as shown in Fig. 12.

To connect or disconnect the two receivers, a series-shunt configuration is used, as shown in Fig. 11(a). This configuration improves the isolation between the two receivers in standalone mode, and isolates the input from the parasitic capacitance of this long line. With the switches sized to have 2-Ω on-resistance

(a)

(b)
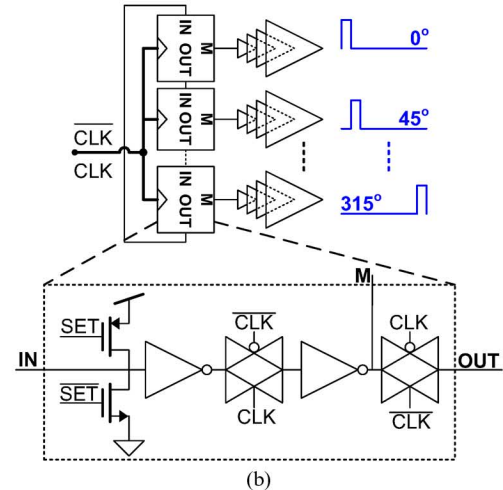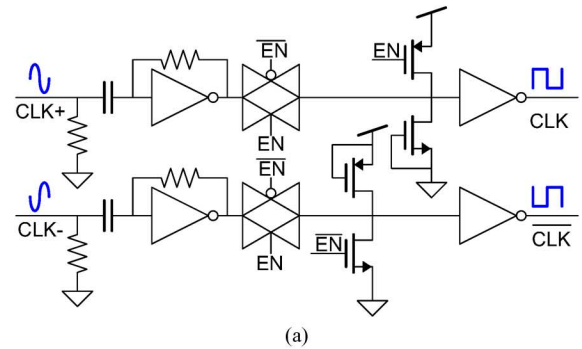
Fig. 10. LO-generation circuitry with: (a) clock input and (b) shift register to generate eight-phase LO.

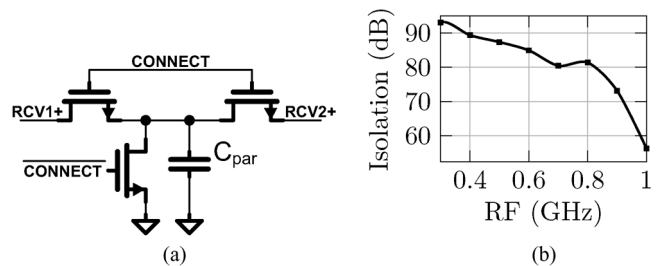(a)   (b)

Fig. 11. Two receivers can be (dis)connected. (a) Circuitry (the negative inputs are connected in an identical way). (b) Isolation measurements.

each, and an ohmic loss of 2 Ω for the wire, 0.5-dB IL is added for the second receiver.

IV. MEASUREMENTS

The chip is implemented in 65-nm low-power CMOS operating at 1.2 V, with an area (including bondpads) of 1×1 mm^2. A photograph is shown in Fig. 12. The active area excluding decap is 0.15 mm^2.

When the receivers are used standalone, they should be sufficiently isolated. With both receivers connected on-chip, both with 0-dB attenuation and in 100-Ω mode, we measured the output power of the second receiver for a certain input power applied to the RF input of the first receiver. We then disconnected both receivers and put them in 50-Ω mode (again at 0-dB attenuation), again measuring the output power of the second receiver for the same input power applied to the first receiver. The power
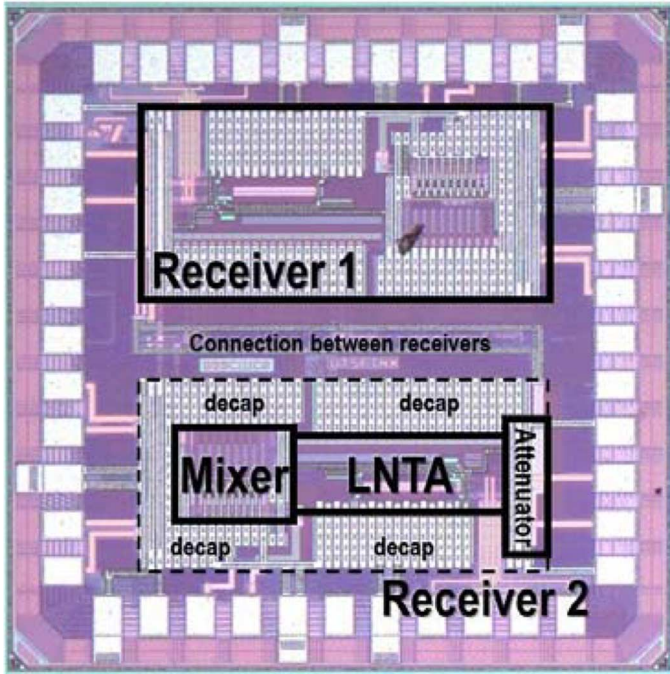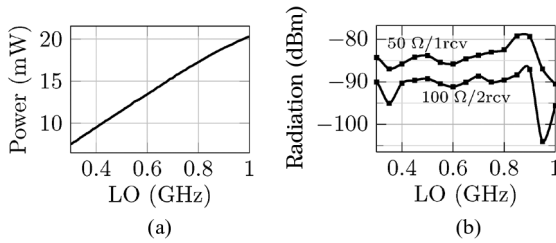
Fig. 12. Chip micrograph.

Fig. 13. Measurements of: (a) power consumption of the LO circuitry and clock drivers and (b) LO radiation at the antenna in the two matched modes.
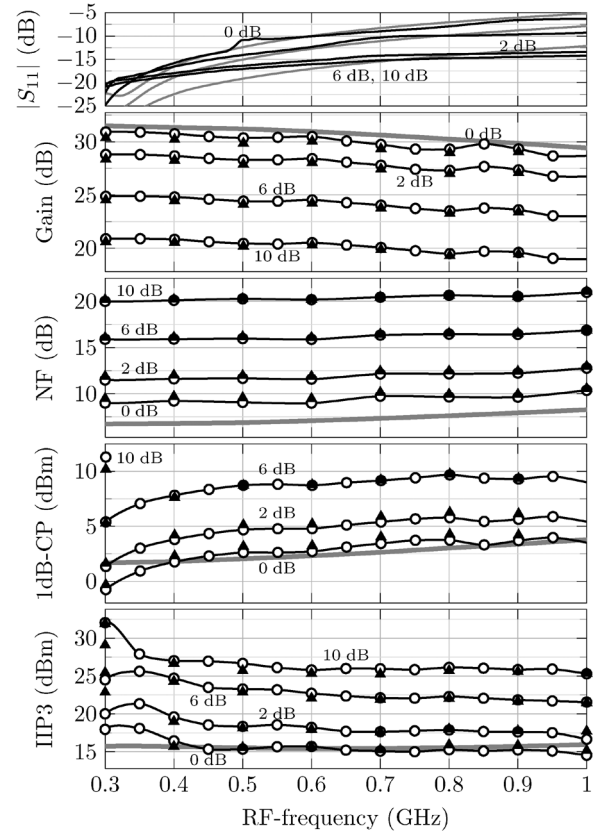

Fig. 14. Measurement results of two receivers in parallel for all attenuation settings (black lines and circles for receiver 1; triangles for receiver 2). Some simulation results are shown as gray lines.

difference between these two measurements shows the isolation between the receiver inputs when they are disconnected, and the result is shown in Fig. 11(b). More than 80 dB of isolation is obtained up to 0.8 GHz, after which it drops to just below 60 dB at 1 GHz.

Fig. 13(a) shows the power consumption of the LO circuitry per receiver: it scales almost linearly from 7.5 mW at $f_{LO} = 0.3$ GHz to 20.4 mW at $f_{LO} = 1.0$ GHz. The differential implementation makes sure that LO leakage from the mixer to the input is low, and the LNTA and attenuator further attenuate this. The measured LO radiation (0-dB attenuation) is shown in Fig. 13(b) and is well below -70 dBm, and scales with the attenuation (not shown), as expected. The on-chip RF circuitry consumes 15.3/12.8/10.3 mW per receiver in the 50-Ω/100-Ω/highZ mode.

In the following measurements, the IL of cables and hybrid, but not the PCB, have been corrected for in the measurement results; off-chip baseband circuitry is not de-embedded. The feedback resistance of the TIA is 1 kΩ, and the feedback capacitance is 8 pF for 20-MHz bandwidth. The antialias filters have a cutoff frequency of 8 MHz, and the ADCs sample at 10 MSa/s, resulting in a noise floor that is slightly higher near the Nyquist frequency in digital baseband due to aliasing.

A. Two Receivers in Parallel

Measurement results of two receivers in parallel, each with 100-Ω input impedance, are shown in Fig. 14. Matching ($S_{11} < -9.6$ dB) at 0-dB attenuation is obtained from 150 MHz (limited by the external inductor) to 650 MHz (limited by capacitance of the attenuators, LNTAs, four bondpads, and the long interconnect). At higher attenuation, the inductor and a large part of the capacitance is shielded by the resistive attenuator so that matching is achieved from below 100 MHz to above 1 GHz.

At 0-dB attenuation, the gain is around 30 dB, and varies 2.2 dB over the whole band, which closely matches simulation. The NF is around 10 dB, which is almost 3 dB more than simulated. Even after extensive searching and debugging, the cause of this discrepancy has not been found. The gain (NF) of the other receiver follows that of the first, but is 0.2–0.6 dB lower (higher) as expected. The gain curves are lowered by the attenuation, and maintain the same shape.

At 0-dB attenuation, the 1-dB compression point (CP) increases from 0 dBm at 300 MHz to around $+3$ dBm at 700 MHz and above. IIP$_3$ is very close to simulation results at around $+15$ dBm over the whole band, except below 400 MHz where it is a bit higher. Both CP and IIP$_3$ increase 1 dB per dB with the attenuation (CP at 10-dB attenuation is above $+12$ dBm; we did not raise the input power further due to risk of oxide/junction breakdown).
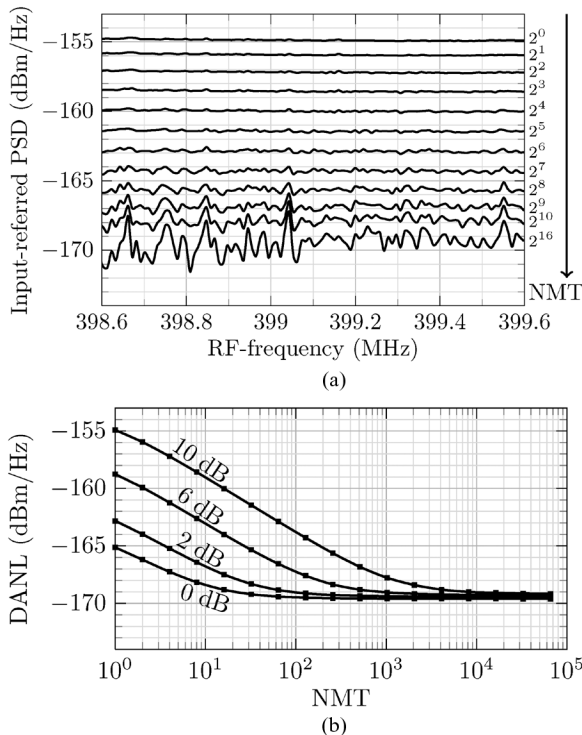
Fig. 15. Crosscorrelation noise measurements at $f_{LO} = 400$ MHz. (a) Noise floor as function of NMT (10-dB attenuation). (b) $DANL_{Hz}$ as function of NMT for all settings.

B. Crosscorrelation

Fig. 15(a) shows the measured noise floor as a function of NMT for 10-dB attenuation at $f_{LO} = 400$ MHz, where NMT = 1 equals the time required to obtain enough samples for one FFT per receiver [100 μs for the 10-kHz RBW in Fig. 15(a)]. The DANL at NMT = 1 is about 1 dB less than what would be expected from Fig. 14. This is because we look at the expected value of the absolute value of the accumulator output, and not at the noise power at the output of a single receiver [3].

For an RBW of 1 MHz, obtaining enough samples for each FFT (independent of the actual ADC sample rate) takes 1 μs. From Fig. 15, $DANL_{Hz}$ decreases from -155 to -167 dBm/Hz after 600 FFTs (for 10-dB attenuation), improving SFDR by 8 dB, which takes only 0.6 ms, an acceptable time for many purposes.

Fig. 16 shows the final $DANL_{Hz}$ after crosscorrelation, measured by inserting a known tone of low power at 1-MHz IF and determining the noise floor around -1-MHz IF (the IF gain at 1 MHz is the same as at -1 MHz). Although the receiver NF is almost 3 dB more than expected, it seems to contribute mainly independent noise in each receiver, as the $DANL_{Hz}$ obtained with crosscorrelation is close to the predicted -172 dBm/Hz.

Fig. 17 shows the measured spectrum of a modulated multitone signal that was applied to the input of the system. As a reference, the spectrum as detected by the individual receivers is also shown. The spectral widening due to nonlinearity in the signal generator can be observed much more clearly and with greater accuracy in the crosscorrelation output.

In the presented system, the oscillators are external with good phase-noise performance, which prohibits a visible improvement in phase noise performance using our ADC board. There-
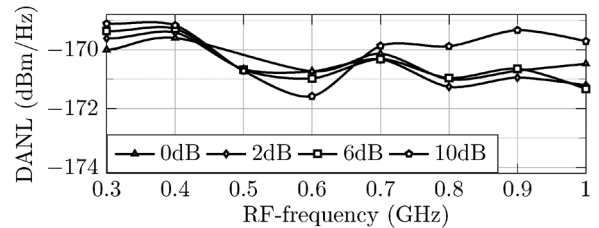

Fig. 16. Final $DANL_{Hz}$ obtained after NMT = 2^{16} as a function of RF frequency and attenuation setting.
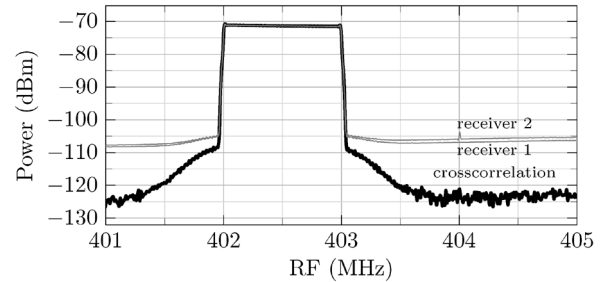

Fig. 17. Output of our SA (10-dB attenuation) when the input contains a modulated 1-MHz-wide 100-multitone signal. The spectra of the individual receivers are also shown.
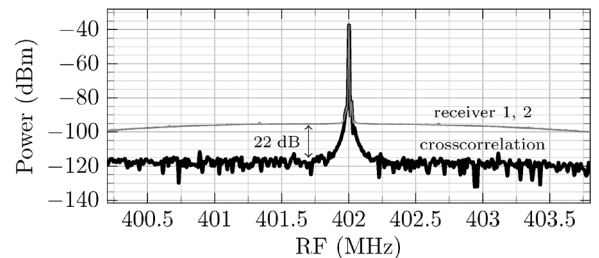

Fig. 18. Measurement results for phase noise reduction using two PM-modulated frequency-locked oscillators (at 0-dB attenuation).

fore, wideband PM modulation is applied to two frequency-locked synthesizers from Agilent Technologies. In this way, the phase noise of both LOs is independent and detectable. The obtained spectra at 0-dB attenuation are shown in Fig. 18. As a reference, the spectra of the individual receivers are also shown. The phase noise is seen to be reduced by more than 20 dB. This improvement is independent of the actual phase noise performance of the LOs so it can also be used to make a good LO look even better.

C. Single Receiver

With the receiver used for regular reception, the two receivers are disconnected on-chip, as described in Section III-D. Each receiver turns to 50-Ω input impedance by reconfiguring the attenuator and LNTA, as described in Sections III-A and III-B. The results are shown in Fig. 19. They are in many ways comparable to the two-receiver case, which is why we only briefly mention some differences here.

Disconnecting the receivers largely reduces the parasitic capacitance at the input, which results in a much wider matching bandwidth. With two CG transistors turned on for 50-Ω matching, the transconductance of the LNTA is expected to increase by about 1 dB, which is verified in the measurements. Due to the lower capacitance, the gain curve is more constant than for two receivers. The NF at 0-dB attenuation
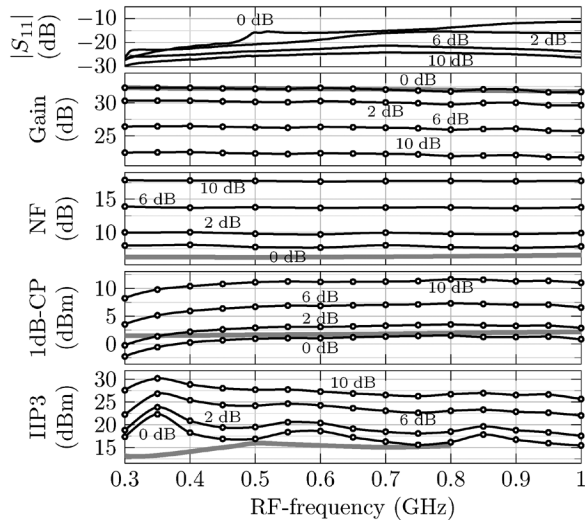
Fig. 19. Measurement results of a single receiver for all attenuation settings. Some simulation results are shown as gray lines.
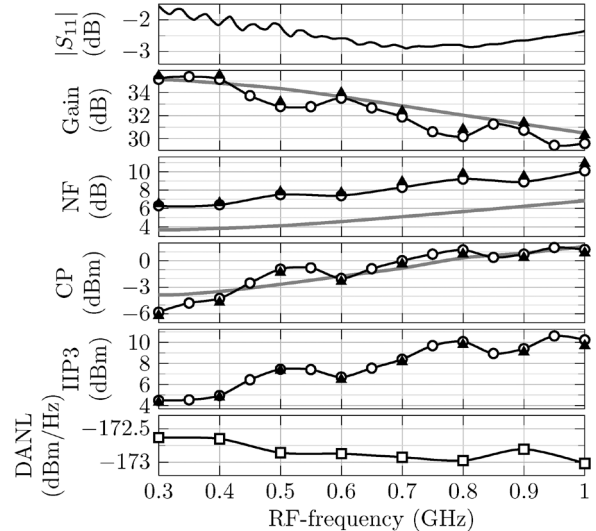

Fig. 20. Measurement results of two receivers in parallel with high-ohmic inputs (squares for receiver 1, triangles for receiver 2). Some simulation results are shown as gray lines.

is measured at around 8 dB, which is again almost 3 dB more than simulated. Compared to the two-receiver case, CP is lower by about the same amount as the gain is higher. IIP_3, on the other hand, is very comparable, which is in agreement with Fig. 9. It is likely that IIP_3 does not follow CP because there is some distortion canceling in the LNTA, which only works in the small-signal regime.

D. High-Impedance Mode

The noise correlation, which limits the measured DANL_{Hz} to about -171 dBm/Hz (see Fig. 16) is due to the matching at the input. The inputs of the receivers can be made high ohmic so that, in principle, no noise currents can flow from one receiver to the other. This should not only obtain a higher sensitivity [6], [15], but is also very interesting for BIST, where internal nodes are preferably not loaded.

The measurement setup is exactly the same as for the matched case. IL corrections due to wiring and the external hybrid are corrected up to the input of the PCB *with the integrated circuit (IC) matched*. We model the source (signal generator) as a voltage source with 50-Ω output resistance. The signal generator assumes 50-Ω matching, and can be modeled as a voltage source with 50-Ω output impedance. It generates twice the voltage required for the desired power at a 50-Ω load. With the cables and hybrid also matched to 50 Ω, the high-ohmic setting of the IC will produce double the voltage compared to the matched setting for the same source voltage. Since the MOS devices are voltage controlled, this passive voltage gain improves measured gain and NF. Similarly, the higher voltage swing degrades IIP_3 and CP.

The transfer of the used hybrid (Tyco H-183-4) is not specified for terminations other than 50 Ω, and its effect is not de-embedded. The measurement results, shown in Fig. 20 for two high-ohmic receivers in parallel, agree reasonably well with simulations with an ideal hybrid. Note that resistive attenuation does not make sense in this case, and thus only the 0-dB setting is measured.

The measured return loss is less than 3 dB over the whole band; most of the power is reflected, as desired. At higher frequencies, parasitic input capacitance lowers the gain and increases the NF. As one would expect, compression and linearity curves also follow the gain curve.

Ideally, there will be *no* correlated noise in the two receivers, and the DANL_{Hz} after correlation should be close to -174 dBm/Hz. The measurements indicate that this is almost achieved: we measure a DANL_{Hz} around -173 dBm/Hz, again about 1 dB higher than predicted in Section III-B. Apart from small calibration errors, this difference may be explained by the shared low-ohmic ground that may introduce some noise correlation, and the IL of the PCB, which directly translates to a higher DANL.

V. BENCHMARKING

It is very hard to properly compare SAs because there are so many different aspects to consider. Therefore, we limit ourselves here to DANL and IIP_3. Table I compares a number of SAs, spectrum sensing solutions, and wideband receivers from literature with our work. For the SAs, we have taken the values given at 0-dB attenuation and without any (optional) preamplifiers turned on. For the integrated solutions, we have converted reported NF or sensitivity values to DANL_{Hz}. For NF, we use $\text{DANL}_{\text{Hz}} = \text{NF} - 174$ (dBm/Hz), and for sensitivity, DANL_{Hz} is set equal to the sensitivity in dBm/Hz. For our work, we have included three cases: 0-dB attenuation, 10-dB attenuation, and the highZ mode.

Without crosscorrelation, the linearity and DANL are comparable with commercial SAs. With crosscorrelation, however, we obtain a significantly lower noise floor, even lower than the PXA with NFE enabled. Note that lowering the noise floor comes at the cost of measurement time. The 10-dB attenuation setting requires 1700 averages to get a DANL_{Hz} of -168 dBm. Due to a lower NF for the same IIP_3, this is 2.5 times faster than a previously presented more discrete prototype [3]. Even though the NFE in the PXA seems to be reducing the noise floor by 8 dB

TABLE I
COMPARISON WITH IMPLEMENTATIONS FROM LITERATURE AND STATE-OF-THE-ART COMMERCIAL SAs
(TYPICAL VALUES AT 0-dB ATTENUATION; PRE-AMPLIFIER OFF)

	Remarks [a]	Frequency Low (MHz)	Frequency High (GHz)	Power (mW)	IIP3 (dBm)	DANL$_{Hz}$ (dBm/Hz)	Improved DANL$_{Hz}$ (dBm/Hz)[b]	Time penalty [c]	SFDR in 1 MHz RBW (dB)[d]
This work, 0 dB	C65	300	0.7	41–54	15	-163	-169	16	83
This work, 10 dB	C65	300	1.0	41–66	25	-153	-169	$1.7 \cdot 10^3$	89
This work, highZ	C65	300	1.0	36–61	5	-164	-172	42	78
[3]	D+C65	50	1.5	191	24	-141	-169	$4.3 \cdot 10^3$	89
[16]	C180	400	900	180	-17	-124			31
[11]	C90	30	2.4	30–44	8	-135			55
[12]	C40	80	2.7	35–78	-22[e]	-172			72
[13] (maximum gain)	C80	40	1.0	440	-15	-171			64
Agilent PXA-N9030A	B	0	3.6	$450 \cdot 10^3$	22	-154	-162	40	83
CRFS RFeye Node	M	10	6.0	$15 \cdot 10^3$	20	-164			83
Rohde & Schwarz FSH4	H	0.01	3.6	$12 \cdot 10^3$	15	-145			67

[a] B: commercial benchtop, C: CMOS, D: discrete components, H: commercial handheld, M: commercial outdoor monitoring

[b] After crosscorrelation (for the PXA: with NFE enabled)

[c] Additional time required to get within 1 dB of the final DANL

[d] Taking into account only (improved) DANL and IIP$_3$

[e] Not stated in [12], but obtained from personal communication with the author

immediately (calibration of the noise level is done at start-up, which takes some time), the variance is still the same as at the level of -154 dBm/Hz. It takes an estimated 40 averages to get a variance that belongs to a -162-dBm/Hz noise level.

Compared to spectrum sensing solutions in literature, we obtain a much higher linearity and better DANL, even without crosscorrelation. Note that [11]–[13] and [16] also have integrated baseband components so the comparison may not be entirely fair. Nevertheless, it still gives an indication that the performance achieved by this technique is very promising.

VI. CONCLUSIONS

An integrated SA is desirable for SDR, dynamic spectrum access, and BIST, but the design faces many challenges. Spectrum analysis using crosscorrelation, which requires the use of two receivers, can reduce thermal noise and phase noise, and improve linearity, at the cost of measurement time. This enables the design of an integrated SA with high-performance metrics. In this work, we have shown a high-linearity design in 65-nm CMOS, which operates at 1.2 V from 300 MHz to 1.0 GHz. It achieves $+25$ dBm IIP$_3$ and a DANL$_{Hz}$ of better than -169 dBm/Hz at a power consumption of around 50 mW. When matching is not required, the DANL$_{Hz}$ can be reduced even further to below -172 dBm/Hz.

Based on the results obtained, we conclude that crosscorrelation with two linear frontends is promising to realize integrated SAs in CMOS with high linearity and sensitivity.

ACKNOWLEDGMENT

REFERENCES

[1] P. F. Marshall, "Dynamic spectrum management of front end linearity and dynamic range," in *Proc. 3rd IEEE New Frontiers Dynam. Spectr. Access Netw. Symp.*, 2008, pp. 1–12.

[2] D. T. Lin, C. Hyungil, L. Li, and M. P. Flynn, "A 600 MHz to 3.4 GHz flexible spectrum-sensing receiver with spectrum-adaptive reconfigurable DT filtering," in *Proc. IEEE Radio Freq. Integr. Circuits Symp.*, Jun. 17–19, 2012, pp. 269–272.

[3] M. S. Oude Alink, E. A. M. Klumperink, A. B. J. Kokkeler, M. C. M. Soer, G. J. M. Smit, and B. Nauta, "A CMOS-compatible spectrum analyzer for cognitive radio exploiting crosscorrelation to improve linearity and noise performance," *IEEE Trans. Circuits Syst. I, Reg. Papers*, vol. 59, no. 3, pp. 479–492, Mar. 2012.

[4] M. S. Oude Alink, E. A. M. Klumperink, A. B. J. Kokkeler, W. Cheng, Z. Ru, A. Ghaffari, G. J. M. Wienk, and B. Nauta, "A CMOS spectrum analyzer frontend for cognitive radio achieving $+25$ dBm IIP3 and -169 dBm/Hz DANL," in *Proc. IEEE Radio Freq. Integr. Circuits Symp.*, Montreal, QC, Canada, Jun. 17–19, 2012, pp. 35–38.

[5] R. Tandra and A. Sahai, "Fundamental limits on detection in low SNR under noise uncertainty," in *Proc. Int Wireless Netw., Commun., Mobile Comput. Conf.*, 2005, vol. 1, pp. 464–469.

[6] M. S. Oude Alink, A. B. J. Kokkeler, E. A. M. Klumperink, G. J. M. Smit, and B. Nauta, "Lowering the SNR wall for energy detection using cross-correlation," *IEEE Trans. Veh. Technol.*, vol. 60, no. 8, pp. 3748–3757, Oct. 2011.

[7] "FSUP Quick Start Guide," Rohde & Schwarz, Munich, Germany, Jan. 2008.

[8] M. S. Oude Alink, A. B. J. Kokkeler, E. A. M. Klumperink, Z. Ru, W. Cheng, and B. Nauta, "Improving harmonic rejection for spectrum sensing using crosscorrelation," in *Proc. Eur. Solid-State Circuits Conf.*, Bordeaux, France, Sep. 17–21, 2012, pp. 361–364.

[9] Z. Ru, N. Moseley, E. Klumperink, and B. Nauta, "Digitally enhanced software-defined radio receiver robust to out-of-band interference," *IEEE J. Solid-State Circuits*, vol. 44, no. 12, pp. 3359–3375, Dec. 2009.

[10] W. Cheng, M. S. Oude Alink, A. J. Annema, G. J. M. Wienk, and B. Nauta, "A wideband IM3 cancellation technique for CMOS attenuators," in *Proc. IEEE Int. Solid-State Circuits Conf. Tech. Dig.*, San Francisco, CA, Feb. 19–23, 2012, pp. 78–79.

[11] M. Kitsunezuka, H. Kodama, N. Oshima, K. K. , M. T. , and M. Fukaishi, "A 30-MHz–2.4-GHz CMOS receiver with integrated RF filter and dynamic-range-scalable energy detector for cognitive radio systems," *IEEE J. Solid-State Circuits*, vol. 47, no. 5, pp. 1084–1093, May 2012.

[12] D. Murphy, A. Hafez, A. Mirzaei, M. Mikhemar, H. Darabi, M. Chang, and A. Abidi, "A blocker-tolerant wideband noise-cancelling receiver with a 2 dB noise figure," in *Proc. IEEE Int. Solid-State Circuits Conf. Tech. Dig.*, San Francisco, CA, Feb. 19–23, 2012, pp. 74–76.

[13] J. Greenberg, F. De Bernardinis, C. Tinella, A. Milani, J. Pan, P. Uggetti, M. Sosio, S. Dai, S. Tang, G. Cesura, G. Gandolfi, V. Colonna, and R. Castello, "A 40 MHz-to-1 GHz fully integrated multistandard silicon tuner in 80 nm CMOS," in *Proc. IEEE Int. Solid-State Circuits Conf. Tech. Dig.*, San Francisco, CA, Feb. 19–23, 2012, pp. 162–164.

[14] F. Bruccoleri, E. Klumperink, and B. Nauta, "Wide-band CMOS low-noise amplifier exploiting thermal noise canceling," *IEEE J. Solid-State Circuits*, vol. 39, no. 2, pp. 275–282, Feb. 2004.

[15] C. Ciofi, F. Crupi, and C. Pace, "A new method for high-sensitivity noise measurements," *IEEE Trans. Instrum. Meas.*, vol. 51, no. 4, pp. 656–659, Aug. 2002.

[16] J. Park, T. Song, J. Hur, S. M. Lee, J. Choi, K. Kim, K. Lim, C.-H. Lee, H. Kim, and J. Laskar, "A fully integrated UHF-band CMOS receiver with multi-resolution spectrum sensing (MRSS) functionality for IEEE 802.22 cognitive radio applications," *IEEE J. Solid-State Circuits*, vol. 44, no. 1, pp. 258–268, Jan. 2009.

Mark S. Oude Alink (S'09) was born in Hengelo, The Netherlands, on June 20, 1984. He received the B.Sc. degree in computer science and M.Sc. degrees in electrical engineering and computer science (both *cum laude*) from the University of Twente (UT), Enschede, The Netherlands, in 2004 and 2008, respectively, and is currently working toward the Ph.D. degree at UT.

He is currently with the Integrated Circuit Design (IC-Design) Group and the Computer Architecture for Embedded Systems Group, UT. His research includes system design, spectrum sensing, and modulation for cognitive radio.

Eric A. M. Klumperink (M'98–SM'06) was born on April 4, 1960, in Lichtenvoorde, The Netherlands. He received the B.Sc. degree from HTS Enschede, Enschede, The Netherlands, in 1982, and the Ph.D. degree from the University of Twente, Enschede, The Netherlands, in 1997. His doctoral thesis was entitled "Transconductance Based CMOS Circuits."

After a short period in industry, in 1984 he joined the University of Twente, where he participated in analog CMOS circuit research. In 1998, he became an Assistant Professor with the Integrated Circuit Design (IC-Design) Laboratory, Twente, The Netherlands. His research focus then changed to RF CMOS circuits. From April to August 2001, he extended his RF expertise during a sabbatical with the Ruhr Universität, Bochum, Germany. Since 2006, he has been an Associate Professor teaching analog and RF IC electronics courses. He participates in the CTIT Research Institute, guiding Ph.D. and M.Sc projects related to RF CMOS circuit design with a focus on SDR, cognitive radio, and beamforming. He has authored or coauthored over 120 international refereed journal and conference papers. He holds several patents.

Dr. Klumperink was an associate editor for the IEEE Transactions on Circuits and Systems—II: Analog and Digital Signal Processing (2006 and 2007), the IEEE Transactions on Circuits and Systems—I: Regular Papers (2008 and 2009), and the IEEE Journal of Solid-State Circuits (since November 2010). He is a member of the Technical Program Committees of the International Solid State Circuits Conference (ISSCC) and IEEE RFIC Symposium. He was a corecipient of the ISSCC 2002 and 2009 Van Vessem Outstanding Paper Award.

André B. J. Kokkeler received the Ph.D. degree from the University of Twente, Enschede, The Netherlands, in 2005. His thesis was entitled "Analog–Digital Codesign using Coarse Quantization."

For over six years, he was a System Engineer with Ericsson. For eight years, he was a Scientific Project Manager with the Netherlands Foundation for Research in Astronomy (ASTRON). In 2003, he joined the University of Twente. He has a background in telecommunication, mixed-signal design, and signal processing. His current main interest lies in the area of applying low-power design techniques for computationally intensive applications. The emphasis is on reconfigurable architectures for streaming applications. He is involved in research projects sponsored by the Dutch and European Governments and industry.

Zhiyu Ru (S'05–M'09) received the B.Eng. degree from Southeast University, Nanjing, China, in 2002, the M.Sc. degree from Lund University, Lund, Sweden, in 2004, and the Ph.D. degree from the University of Twente, Enschede, The Netherlands, in 2009, all in electrical engineering.

In 2003, he was a Design Engineer with Z-Com, where he was involved with WLAN products. In 2004, he did a six-month internship with Ericsson Mobile Platforms (now ST-Ericsson), during which time he was involved with DVB-T receiver systems. From 2005 to 2009, he was a Research Assistant with the Integrated Circuit Design (IC-Design) Group, University of Twente, where he was involved with the subject of SDRs in CMOS. From 2010 to 2012, he was a Postdoctoral Researcher with the University of Twente. He is currently with MediaTek, Woburn, MA.

Wei Cheng was born in Wuhan, Hubei, China, in 1980. He received the B.E. degree in measuring technology and instrumentation from Xiamen University, Xiamen, China, in 2002, and the M.Sc. degree and Ph.D. degree in electrical engineering from the University of Twente, Enschede, The Netherlands, in 2006 and 2012, respectively.

From 2002 to 2003, he was an academic employee with the Department of Mechanical and Electrical Engineering, Xiamen University, Xiamen, China. He is currently with Qualcomm Inc., San Diego, CA. His interest is analog/RF IC design.

Bram Nauta (M'91–SM'03–F'08) was born in Hengelo, The Netherlands. He received the M.Sc. degree (cum laude) in electrical engineering Ph.D. degree from the University of Twente (UT), Enschede, The Netherlands, in 1987, and 1991, respectively. His doctoral research concerned the subject of analog CMOS filters for very high frequencies.

In 1991, he joined the Mixed-Signal Circuits and Systems Department, Philips Research, Eindhoven, The Netherlands. In 1998, he returned to UT, as Full Professor heading the Integrated Circuit Design (IC-Design) Group. His current research interest is high-speed analog CMOS circuits.

Dr. Nauta was an associate editor of the IEEE Transactions on Circuits and Systems—II: Analog and Digital Signal Processing (1997–1999). He was an associate editor (2001–2006) and later the editor-in-chief (2007–2010) of the IEEE Journal of Solid-State Circuits. He is member of the Technical Program Committees of the International Solid-State Circuits Conference (ISSCC), where he is the 2013 Program Committee chair, the European Solid-State Circuit Conference (ESSCIRC), and the Symposium on VLSI Circuits. He is a Distinguished Lecturer of the IEEE. He is an elected member of IEEE Solid-State Circuits Society Administrative Committee (AdCom). He was a corecipient of the ISSCC 2002 and 2009 Van Vessem Outstanding Paper Award.